

STABILITY ANALYSES FOR GEOSYNTHETIC-REINFORCED STEEP-FACED SLOPES SUBJECTED TO TOE SCOURING

Ching-Chuan Huang^{1*}, Bo-Shin Huang², and Yue-Wing Chen²

ABSTRACT

Knowledge on the influence of a scoured slope toe to the stability of earth structures is key to their long-term maintenance and disaster mitigation. As a follow-up of an experimental study on geosynthetic-reinforced steep-faced slopes subjected to toe scouring, limit-equilibrium-based stability analyses were performed to investigate their effectiveness in evaluating the stability of the slope. Results of analyses showed that the safety factors for pull-out, tie-break, facing connection, base sliding, and overturning failures were insensitive to the boundary changes induced by the toe scouring. The toe-scouring-induced instability of the slope was reflected by the reduction of safety factors against bearing capacity and circular sliding. Among the methods used, the circular failure analysis demonstrated the highest versatility and potentiality in detecting the toe-scouring-induced instability of reinforced steep slopes.

Key words: Geosynthetic-reinforced slope, limit equilibrium analysis, toe scouring, internal stability, external stability, circular failure analyses.

1. INTRODUCTION

Results of post-earthquake and post-tsunami site reconnaissance suggested that flawed or scoured slope toe conditions may account for the catastrophic failure of soil structures such as slopes, retaining walls, and sea walls (Huang and Chen 2004, 2005, Yamaguchi *et al.* 2012; Kuwano *et al.* 2014). Results of the site reconnaissance after a devastating tsunami in the 2011 Great East Japan Earthquake in Japan indicated that catastrophic failures of coastal dykes might have been initiated by overflow-induced scouring at the toe of the downstream slope (Yamaguchi *et al.* 2012 and Kuwano *et al.* 2014). As a result of these post-tsunami studies, a steep-faced geosynthetic-reinforced soil dyke was proposed by Yamaguchi *et al.* (2012). In contrast to the above-mentioned natural forces, human activities such as excavations also play a role in destabilizing natural or manmade slopes, causing landslides (Guadagno *et al.* 2005). Huang (2015) proposed a technique of reinforced earth slab using two layers of reinforcement to mitigate possible excessive settlement of a footing at the crest of the slope. El-Eman and Bathurst (2004, 2007) showed the importance of toe-restraining conditions to the seismic displacement and lateral earth pressure distributions of steep-faced geosynthetic-reinforced soil retaining walls based on the results of model tests. Tatsuoka *et al.* (2007) and Huang *et al.* (2008) performed experimental and analytical studies on using soil bags with integrated reinforcement strips as the facing of reinforced slopes to enhance the stability of earth dams against over-flow-induced scouring and instability. Huang and Chen (2012a, b) investigated the stability and deformation of geosyn-

thetic-reinforced vertically faced soil retaining walls subjected to simulated toe scouring. Results of limit equilibrium analyses performed by Huang and Chen (2012a, b) showed that to avoid catastrophic failures of the wall subjected to toe scouring, the required safety factors against internal failures should be moderately increased. In general, experimental and/or analytical works exploring the stability and deformation characteristics of reinforced soil slopes (or retaining wall) subjected to a progressive loss of the support at the slope toe are limited (*e.g.*, Miyata *et al.* 2015, Huang and Chen 2012a, b). Investigations on the failure mechanism of reinforced slopes subjected to toe scouring are performed based on the results of a series of model tests using limit-equilibrium-based stability analyses to gain new knowledge on the behavior of steep-faced reinforced slopes with a scoured toe.

2. MODEL TEST FACILITY AND TEST RESULTS

The model test system consists of a steel frame of 2.5 m-long, 1.0 m-wide, and 0.15 m-thick for containing a 433 mm-high idealized two-dimensional slopes. Stainless steel rods with a uniform diameter of 1.96 mm and a length of 150 mm were stacked in a rhombic pattern having a unit weight of $\gamma = 68.5 \text{ kN/m}^3$ which is approximately 4 times that of a typical soil ($\gamma = 17 \text{ kN/m}^3$), simulating a stress level of a 4-g condition (g : gravitational acceleration), *i.e.*, a similar stress level in a 1.7 m-high (= 0.433 m \times 4) slope is achieved in the model slopes. Other details of the model slope were reported by Huang (2015). The facing of steep reinforced slope was jointed with 10 load cells which are capable of measuring normal and shear forces simultaneously with a negligibly small coupling effect which has been reported in-detail by Huang and Chen (2012a). Displacement sensors were installed at various locations to measure the displacement of facing and the settlement at the crest of the slope, as shown by Disp1 ~ Disp8 in Fig. 1.

Manuscript received February 23, 2016; revised July 1, 2016; accepted July 3, 2016.

¹ Professor (corresponding author), Department of Civil Engineering, National Cheng Kung University. No. 1, University Rd., Tainan, Taiwan (e-mail: samhc@mail.ncku.edu.tw).

² Graduate Student, Department of Civil Engineering, National Cheng Kung University. No. 1, University Rd., Tainan, Taiwan.

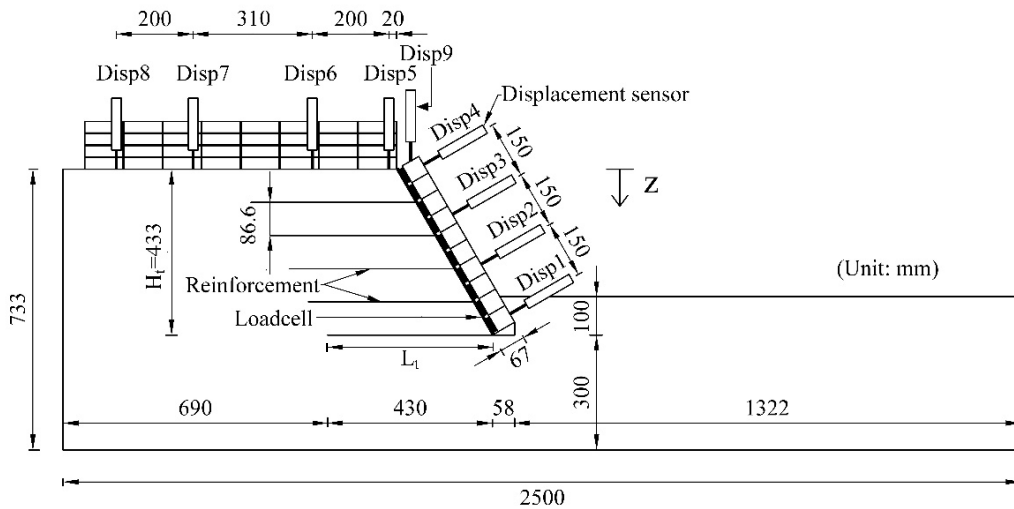


Fig. 1 Geometry of model test facility

The internal friction angle (ϕ) of the steel rod assembly has curved Mohr-Coulomb failure envelope, expressed as $c = 0$ kPa, and ϕ as a function of effective confining stress (σ_n), based on the result of a medium-scale direct shear tests using a 105 mm-long, 100 mm-high (upper + lower boxes), and 150 mm-wide shear box:

$$\phi = 40.9^\circ - 30.2^\circ \times \log(\sigma_n / \sigma_{n0}) \quad (1)$$

where

- σ_{n0} : reference confining stress (= 18.25 kPa)
- σ_n : confining stress in the range of 18.25 ~ 50 kPa

In the following stability analyses, three values of internal friction angle were determined based on three different values of overburden pressures (σ_n) corresponding to three depths, namely, depths of 216 mm (= 433 mm / 2), 366 mm (= 733 mm / 2), and 583 mm (= 433 mm + 300 mm / 2). Values of σ_n (including self-weight and surcharge, $q = 10$ kPa) at the above-mentioned depths are 25, 35, and 50 kPa, respectively, which in-turn yield $\phi = 37^\circ$, 32° , and 27° , for lateral pressure, circular failure, and bearing capacity analyses, respectively. Note that in the following, $\phi = 38^\circ$ rather than $\phi = 37^\circ$ is used for lateral pressure (or internal stability) analyses, in order to conform with that used in a similar study performed by Huang and Chen (2012a).

A heat-bonded nonwoven geotextile with an ultimate tensile strength (T_f) of 4.8 kN/m at a breakage strain of 35% is used as reinforcement in the tests of reinforced slopes. The connection between the reinforcement sheets and the facing blocks is referred to as a “high-strength connection (HC)” based on the pull-out tests reported by Huang and Chen (2012a). Large-strain type strain gages (YFLA-20, Tokyosoki Co., Japan) with a strain limit of 10% ~ 15% are attached to the surface of reinforcement sheets to measure the reinforcement strains during the tests. The measured reinforcement strains were then converted to the reinforcement stress based on the results of strain gage calibration which has been reported in-detail by Huang (2015). It is conceivable that an infinite number of the patterns of scouring could be applied to a structure because the process of scouring is dominated by the dynamics of water currents and the geometries of the structure. As a preliminary study, limited configurations of

the scoured patterns were used. Figs. 2(a) and 2(b) schematically show shallow and deep scouring procedures, respectively. Both testing procedures comprise removing 20 mm-thick of the test medium at each step, followed by steepening the slope of the foundation at a rate of 2° /step. Along the planned lines of scouring as shown in Figs. 2(a) and 2(b), steel rods are removed piece-by-piece manually in a top-down manner to simulate a progressive loss of soil particles at slope toe. Removing steel rods in such a manner may not reproduce a scouring process in reality. However, the present study focused on the failure mechanism of the slope with a scoured toe, not on the mechanism of scouring itself. In shallow scouring tests, a maximum cutting of foundation, D_f is 80 mm which is about 20% of H_r (= 433 mm; H_r : The full height of the reinforced slope). In deep scouring tests, a maximum value of $D_f = 300$ mm which is about 70% of H_r .

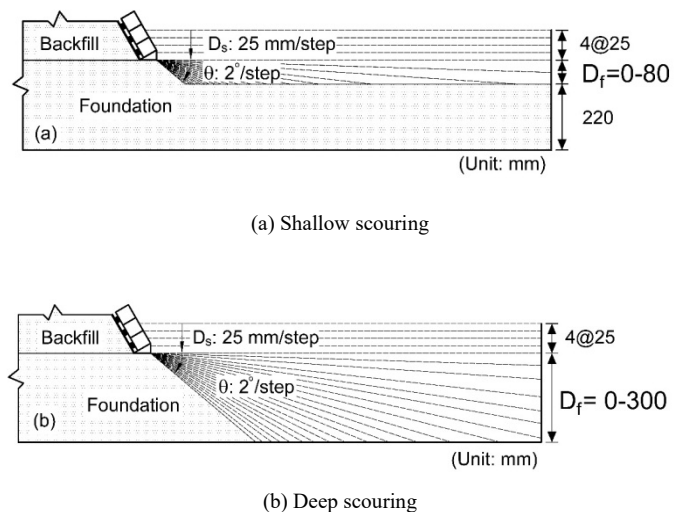


Fig. 2 Schematic scouring procedures

3. OBSERVED FAILURE MECHANISMS

Four model tests are performed and the test results are analyzed here. The test conditions, including L_r / H_t (L_r : Length of reinforcement), ratios between the total reinforcement area and the facing area, and the angle of scoured slope at ultimate failure states (θ_f) are summarized in Table 1. These tests are selected in the present study because of the reinforcement configurations ($L_r / H_t = 0.7$ and 1.0) are of practical significance. Figure 3(a) shows a side-view of an intact slope ($L_r / H_t = 0.7$) before testing. A side-face of the 2-D backfill is marked with white horizontal lines to facilitate the observation of failure mechanisms. Lines are also marked to facilitate the scouring test procedure. Figure 3(b) show the slope at a scoured slope angle of $\theta = \theta_f = 40^\circ$. It can be seen that local shear planes, in the sequence of ‘1’ to ‘4’ appeared in the lower part of the reinforced zone, as a pre-warning of ultimate collapse. Figure 3(c) shows the slope at the verge of total collapse at $\theta = \theta_f = 57^\circ$. A compound sliding through the unreinforced and the reinforced zone can be observed. The following two typical failure patterns were observed: (1) a bearing capacity failure of facing associated with pull-out of bottom layers of reinforcement (as shown in Fig. 4(a)), and/or a bearing capacity failure of facing associated with intensive shear bands behind the facing (as shown in Fig. 4(b)) occurred exclusively for the slope subjected to a shallow scouring; (2) a compound failure consisting of a bearing capacity failure in sloped foundation and/or a global sliding scouring (as shown in Figs. 4(c) and 4(d)).

4. OBSERVED SLOPE DISPLACEMENTS

Figure 5 shows the vertical displacements measured at the top of facing during the process of surcharging and horizontal scouring expressed using a ratio between the equivalent of the wall (H_e) and the total wall height (H_t) defined as:

$$H_e = H + \frac{q}{\gamma} + D_s \tag{2}$$

where

H : unsupported height of the wall at-completion of the slope (= 333 mm)

q : intensity of surcharge (= 0 ~ 10 kPa)

D_s : depth of horizontal scouring (0 ~ 100 mm)

It can be seen in Fig. 5 that the slopes subjected to shallow scouring have higher values of θ_f than those for the deep scouring, suggesting a significant influence of the depth of scouring (D_f) on the behavior of reinforced slopes. In addition, the slopes subjected to shallow scouring have two-step displacement curves as a result of possible stress re-distributions before the ultimate collapse.

5. MEASURED REINFORCEMENT FORCES

Figures 6(a) compare the effect of scouring patterns on the distributions of reinforcement forces measured at $\theta = 40^\circ$ for the slopes using $L_r = 330 \text{ mm} = 0.7H_t$. At $\theta = 40^\circ$, similar reinforcement force intensities and distributions were obtained regardless of the types of scouring. However, distinctively large

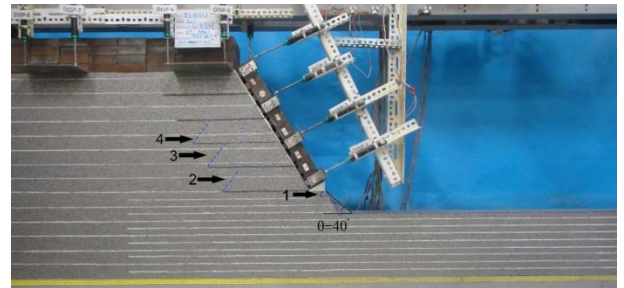
Table 1 Effects of reinforcement lengths on the ultimate collapse states of reinforced slopes subjected to shallow and deep scouring ($q = 10 \text{ kPa}$)

Test	Scouring type	Reinforcement length (L_r / H_t)	Reinforcement area / facing area	Failure state
TE30	Deep scouring	300 mm (0.7)	3.0	$\theta_f^{(1)} = 40^\circ$
TE30(2)	Shallow scouring	300 mm (0.7)	3.0	$\theta_f^{(1)} = 57^\circ$
TE43	Deep scouring	430 mm (1.0)	4.3	$\theta_f^{(1)} = 40^\circ$
TE43(2)	Shallow scouring	430 mm (1.0)	4.3	$\theta_f^{(1)} = 69^\circ$

⁽¹⁾ θ_f denotes the angle of the scoured foundation slope at which a total failure is observed.



(a) Before scouring



(b) Local shear planes observed in sequence of 1-4 at sloped scouring of $\theta = 40^\circ$



(c) At ultimate failure state ($\theta = \theta_f = 57^\circ$)

Fig. 3 Typical side-views of model slope (TE30(2); $L_r = 0.7 H_t$)

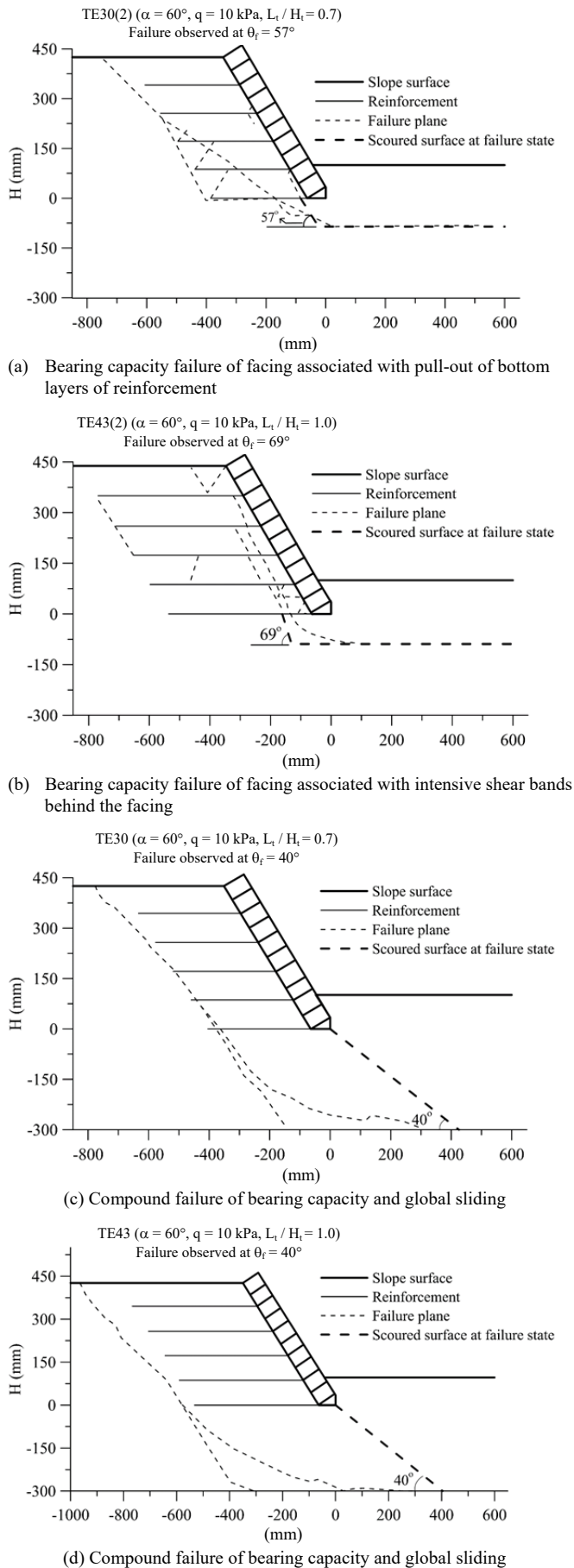


Fig. 4 Summary of observed failure mechanisms

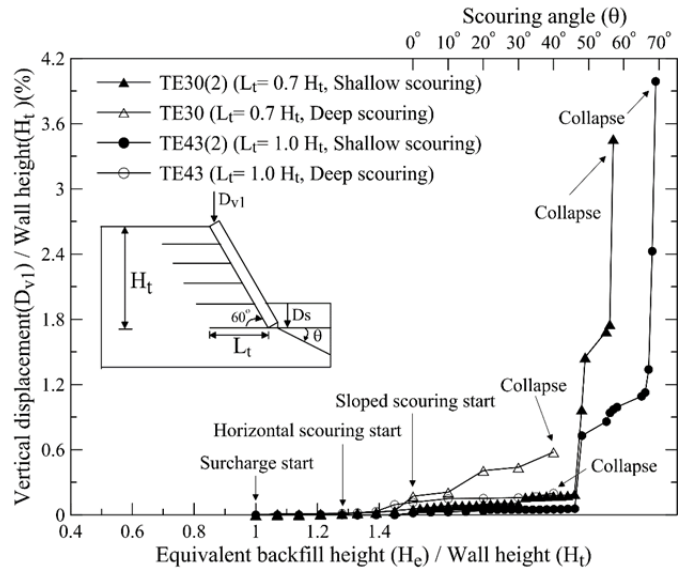


Fig. 5 Settlement measured at the crest of facing during surcharging and scouring

reinforcement forces were measured at $\theta = \theta_f = 57^\circ$ for the case of shallow scouring suggesting that the reinforcement forces mobilized more effectively in shallow scouring case than did the deep scouring. Figure 6(b) shows the distributions of measured reinforcement forces for the slopes using $L_t = 1.0 H_t$. The effect of scouring patterns on the distributions of reinforcement forces at $\theta = 40^\circ$ for tests TE43 and TE43(2) is rather small. It is also noted that at the moment of ultimate collapse, significantly higher reinforcement forces can be found in the case of shallow scouring (at $\theta = \theta_f = 69^\circ$) than those in deep scouring (at $\theta = \theta_f = 40^\circ$). The significantly increased reinforcement forces for lower layers of reinforcement observed at $\theta_f = 57^\circ$ in Fig. 6(a) and at $\theta_f = 69^\circ$ in Fig. 6(b) support the failure mechanism observations in Figs. 4(a) and 4(b), *i.e.*, additional tensile forces were mobilized as a result of the pull-out of reinforcement in response to the bearing capacity failure of facing. This observation also agrees well with the two-step settlement of facings prior to the ultimate collapse of the slopes subjected to shallow scouring as discussed for Fig. 5.

6. INTERNAL STABILITY ANALYSES

Figure 7 schematically shows the forces considered in internal stability analyses, *i.e.*, the tie-break and pull-out failures on the potential failure plane and the pull-out (or connection) failure on facing. The safety factor against tie-break failure (FS_t) is defined as:

$$FS_t = \frac{T_f}{K_a \cdot \sigma_v \cdot S_v} \quad (3)$$

where

T_f : ultimate tensile strength of reinforcement
(= 4.8 kN/m)

K_a : Coulomb's active earth pressure coefficient
(= 0.217 for $\phi = 38^\circ$)

σ_v : effective overburden pressure at the level of reinforcing sheets

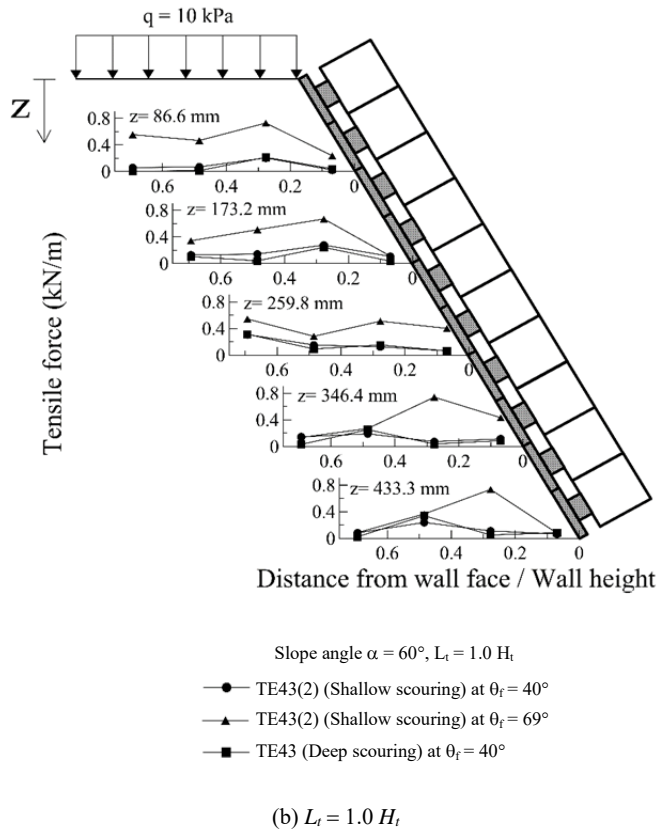
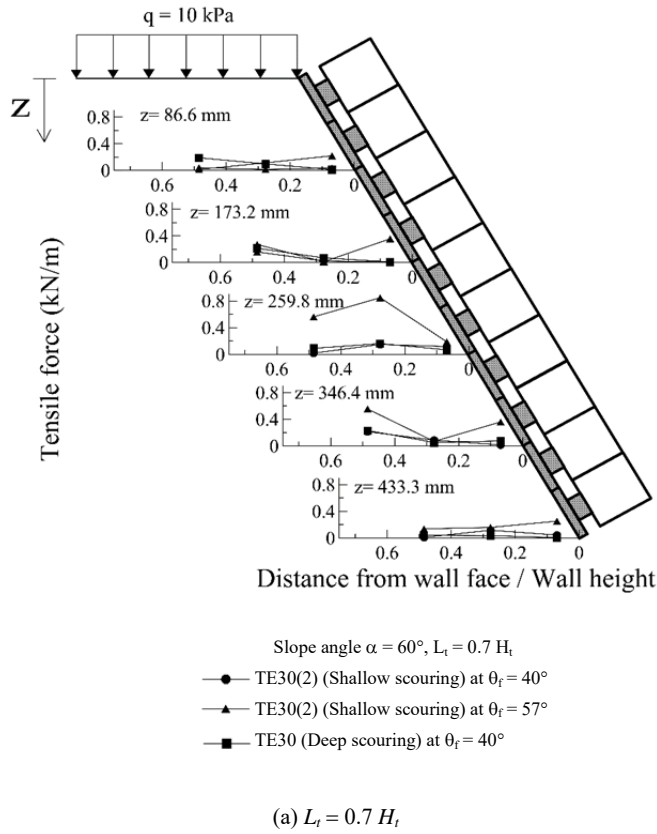


Fig. 6 Comparisons of measured reinforcement force distributions between deep and shallow scouring

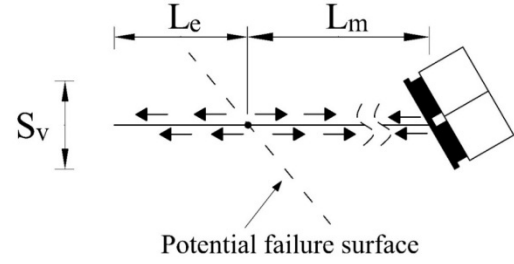


Fig. 7 Schematic view of reinforcement pull-out and tie-break

S_v : tributary height for a certain layer of reinforcement
(= 0.087 m)

The safety factor against pull-out from the stationary zone of backfill (FS_p) is defined as:

$$FS_p = \frac{2 \cdot \sigma_v \cdot \tan \mu \cdot L_e}{K_a \cdot \sigma_v \cdot S_v} \quad (4)$$

where,

μ : soil-reinforcement interface friction angle

L_e : length of embedded reinforcement against pull-out
(as shown in Fig. 7)

The safety factor against facing pull-out (or connection failure), FS_f is defined as:

$$FS_f = \frac{2 \cdot L_f \cdot (c_f + \sigma_v \cdot \tan \phi_f)}{K_a \cdot \sigma_v \cdot S_v} \quad (5)$$

L_f : reinforcement length embedded in facing (= width of facing = 0.05 m)

c_f : cohesion intercept (= 0.7 kN/m) obtained in reinforcement-facing interface pull-out tests reported by Huang and Chen (2012a)

ϕ_f : friction angle (= 60°) obtained in reinforcement-facing interface pull-out tests reported by Huang and Chen (2012a)

Values of FS_t , FS_p , and FS_f calculated for various types of scouring and values of L_t are shown in Figs. 12(a) ~ 12(d) which will be discussed in-detail later.

7. BASE SLIDING AND OVERTURNING FAILURE ANALYSES

The safety factor against base sliding (FS_s) is defined as:

$$FS_s = \frac{P_p \cdot \cos \phi_w + Q_v \cdot \tan \phi_b}{Q_h} \quad (6)$$

$$Q_v = W_1 + W_2 - P_{a1} \sin \phi_w - P_{a2} \sin \phi_w + q \cdot L_t + P_p \cdot \sin \phi_w \quad (7)$$

$$Q_h = (P_{a1} + P_{a2}) \cdot \cos \phi_w \quad (8)$$

where

P_{a1} : active lateral thrust induced by the uniform surcharge
(= $K_a \times q \times H$)

P_{a2} : active lateral thrust induced by the self-weight of backfill ($= 0.5 \times K_a \times \gamma \times H^2$)

P_p : passive lateral thrust induced by the self-weight of backfill in front of the wall ($= 0.5 \times K_p \times \gamma \times D^2$; D : Height of passive zone in front of the facing; $K_p = 9.64$ for $\phi = 38^\circ$)

W_1 : weight of facing

W_2 : weight of reinforced backfill

q : uniform surcharge at the crest of the slope

L_t : total reinforcement length

ϕ_w : interface friction angle could be applied to a structure between reinforced and unreinforced zones ($= \phi/2 = 19^\circ$)

ϕ_b : friction angle at the base of reinforced zone ($= 0.8\phi = 31^\circ$)

The factor safety of overturning around the rotation center (the toe of facing ‘o’ shown in Fig. 9) is defined as:

$$FS_o = \frac{M_r}{M_o} \tag{9}$$

$$M_r = P_p \cos \phi_w L_p + W_1 L_1 + W_2 L_2 + q L_t L_7 \tag{10}$$

$$M_o = P_{a1} \cos \phi_w L_3 + P_{a2} \cos \phi_w L_5 + P_{a1} \sin \phi_w L_6 + P_{a2} \sin \phi_w L_4 \tag{11}$$

where, $L_1, L_2, \dots, L_6, L_t$ and L_p are arms of rotation defined in Fig. 9. The calculated values of FS_s and FS_o for the cases of deep and shallow scouring are summarized in Figs. 12(a) ~ 12(d), respectively, which will be discussed later. Note that to analyze base sliding and overturning failures as schematically shown in Figs. 8 and 9, two types of imaginary boundary lines were used to separate reinforced and unreinforced zones, namely, Type-1: A vertical line passing through point o’ (see Figs. 8 or 9), and Type-2: A line parallel to the facing and passing through point o’. Based on the result of a comparative study using two types of imaginary boundaries, Type-2 was not used in the present study because it yielded: (1) unreasonably large backward eccentricity of resultant reaction force at the base of reinforced zone; (2) higher values of FS_b and FS_o than those obtained using Type-1. This is attributable to: (1) a part of W_2 located to the left of point o’ (see Figs. 8 and 9) transmitting the self-weight to the base (o-o’) when using Type-1 boundary; (2) smaller values of P_{a1} and P_{a2} than those using Type-2 imaginary boundary. Regarding (1), the authors believe that the transmission of that part of self-weight to the base of reinforced zone (o-o’) hasn’t been verified. Therefore, further discussions on Type-2 is beyond the scope of the present study.

8. BEARING CAPACITY FAILURE ANALYSES

The safety factor (FS_b) against bearing capacity failure of a rigid footing placed on a horizontal or sloped ground is defined as (see Fig. 10):

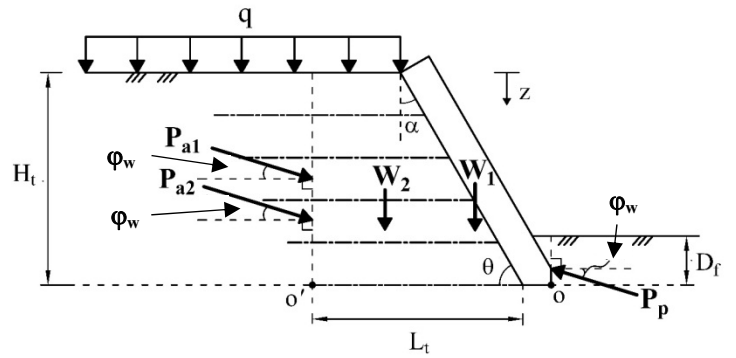


Fig. 8 Forces acting in a reinforced slope for base sliding stability analyses

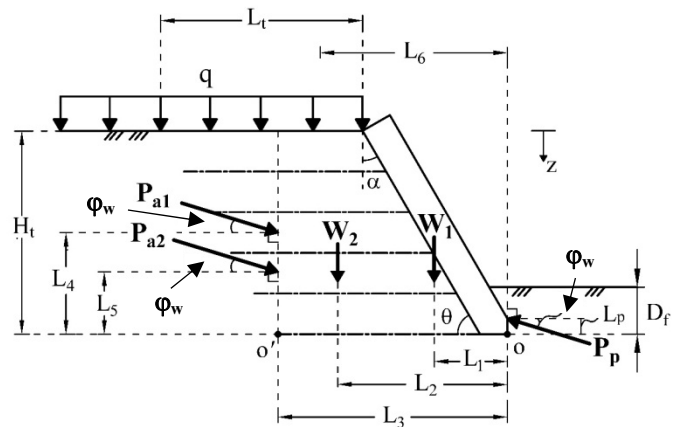


Fig. 9 Forces acting in a reinforced slope for overturning stability analyses

$$FS_b = \frac{q_u}{q_{max}} \tag{12}$$

where q_u is the ultimate bearing capacity of a surface footing calculated using the following equation:

$$q_u = \frac{1}{2} \cdot \gamma \cdot B' \cdot N_\gamma \cdot F_{\gamma\theta} \cdot F_{\gamma\eta} \tag{13}$$

B' : effective footing width ($= B - 2e$; $B(= L_t)$: full width of footing; e : eccentricity of loading at the base of reinforced slope)

N_γ : bearing capacity factor for the self-weight of soil ($= 10$ and 15 suggested by Meyerhof (1963) and Vesic (1973), respectively, for $\phi = 27^\circ$)

$F_{\gamma\theta}$: correction factor for ground inclinations (see Eq. 15 by Hansen 1970; Vesic, 1973, 1975; Huang and Kang 2008)

$F_{\gamma\eta}$: correction factor for load inclinations represented by the angle of load inclination, η (see Eq. 15 by Meyerhof 1963; Huang and Kang 2008)

$$F_{\gamma\theta} = [1 - (1.062 - 0.014 \cdot \phi) \cdot \tan \phi]^{10} \tag{14}$$

$$F_{\gamma\eta} = \left[1 - \left(\frac{\eta}{\phi} \right) \right]^{(0.1\phi - 1.21)} \tag{15}$$

$$\eta = \tan^{-1} \left(\frac{Q_h}{Q_v} \right) \quad (16)$$

The value of q_{\max} is determined using one of the following two equations:

1. Based on Meyerhof's effective width of foundation:

$$q_{\max} = \frac{Q_v}{B'} \quad (17)$$

where

Q_v : total vertical load at the base of reinforced slope

2. Based on the elastic stress distribution at the base of reinforced slope:

$$q_{\max} = \frac{Q_v}{B} \left(1 + \frac{e}{6 \cdot L_f} \right) \quad (18)$$

$$e = \frac{M_o}{Q_v} - \frac{L_f}{2} \quad (19)$$

Values of FS_b during surcharging and simulated toe scouring are summarized in Figs. 12(a), 12(b), 12(c), and 12(d) for tests TE30, TE30(2), TE43, TE43(2), respectively. It can be seen that curves for FS_b showed a slight increase of FS_b during surcharging and a drastic decrease for the 2nd stage (from the beginning of sloped scouring to the ultimate collapse). The 1st segment reflects the increase of q_u due to the application of surcharge (q) at the crest of the slope. The decreased FS_b in the 2nd segment reflects a combined effect of increased slope angles (θ), increased load inclination angles (η), as well as the decrease of B' . It is noted, however, that current knowledge regarding the ultimate bearing capacity as summarized in Eqs. (13) ~ (15) cannot address the effect of the height of the scoured slope (D_s as shown in Figs. 2(a) and 2(b)) to the ultimate bearing capacity of footing. As a result, no difference in the curves of FS_b between deep scouring (Figs. 12(a), 12(c)) and shallow scouring (Figs. 12(b), 12(d)).

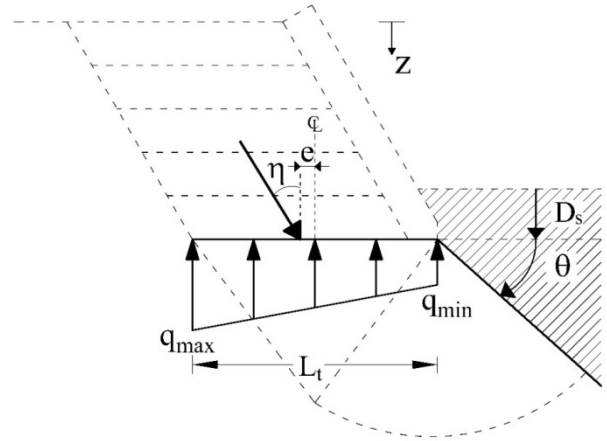


Fig. 10 Schematic view of bearing capacity failure

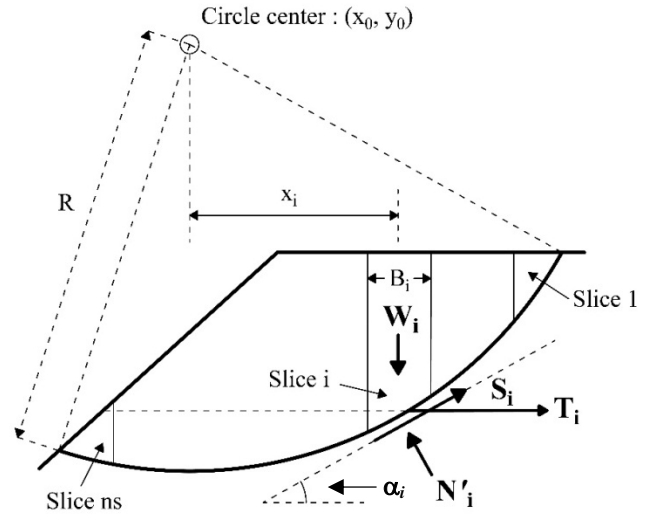


Fig. 11 Schematic view of circular sliding analyses

9. CIRCULAR FAILURE ANALYSES

As a commonly acknowledged definition of safety factor (FS_c) in slope stability analyses:

$$FS_c = \frac{\tau_f}{\tau} \quad (20)$$

τ_f : ultimate strength at the base of slice i according to the Mohr-Coulomb failure criterion

τ : shear stress at the base of slice i

Based on the force equilibrium in the vertical direction, the moment equilibrium and the Mohr-Coulomb failure criterion, Bishop (1955) proposed the following equation of FS_c for a circular failure surface (see Fig. 11):

$$FS_c = \frac{\sum \left[\frac{C_i + (W_i - U_i \cdot \cos \alpha_i) \cdot \tan \phi \cdot \sec \alpha_i}{1 + \left(\frac{\tan \alpha_i \cdot \tan \phi}{FS_c} \right)} \right]}{\sum (W_i \cdot \sin \alpha_i) - \sum (T_i \cdot \cos \alpha_i)} \quad (21)$$

$$C_i = c \cdot l_i = c \cdot B_i \cdot \sec \alpha_i \quad (22)$$

$$U_i = u_i \cdot l_i = u_i \cdot B_i \cdot \sec \alpha_i \quad (23)$$

where

i : slice number ($i = 1, 2, \dots, ns$)

W_i : self-weight of slice i

T_i : Reinforcement force acting at the base of slice i (= 0.45 kN/m based on the averaged value of maximum tensile forces as shown in Figs. 6(a) and 6(b) and the result of preliminary study reported by Huang 2016)

α_i : inclination angle of slice base i

c : cohesion intercept of soil ($c = 0$ in the present study)

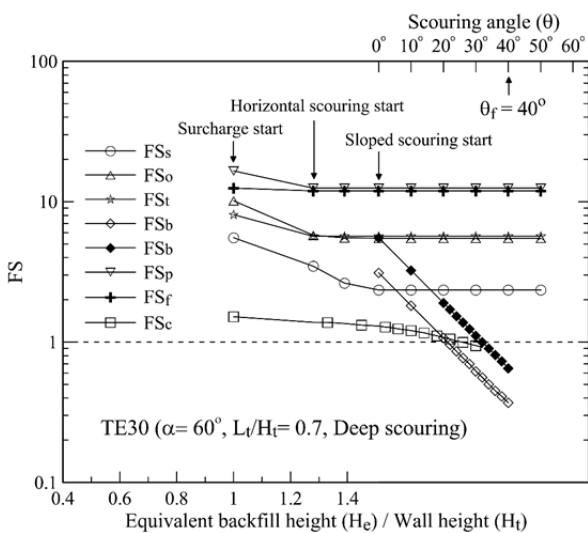
u_i : pore water pressure acting at the base of slice i ($u_i = 0$ in the present study)

l_i, B_i : the length of the base and the width, respectively, for slice i .

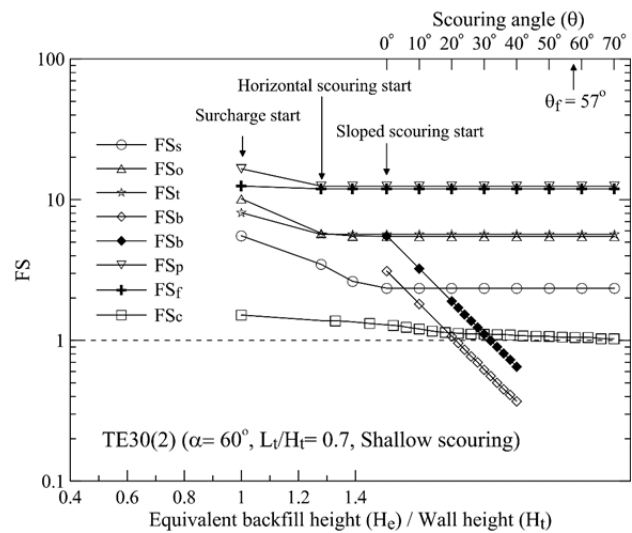
10. RESULTS OF STABILITY ANALYSES

Figures 12(a) ~ 12(d) summarize the results of various stability analyses, in terms of various FS vs. H_e and FS vs. θ relationships. It can be seen that the internal stability analyses (pull-out, tie-break, and facing connection failures) and the external stability analyses (base sliding and overturning) responded insensitively to the change of H_e and θ . Figures 12(a) ~ 12(d) also show that circular (FS_c) and bearing capacity (FS_b) failures dominate the ultimate state of reinforced slopes, regardless of the type of scouring. For bearing capacity analyses, upper and lower bound lines of FS_b are presented. The upper bound of FS_b was derived using Vesic's value of N_γ ($= 15$) in conjunction with the effective footing width B' (Eq. 17); the lower bound was derived using Meyerhof's value of N_γ ($= 10$) in conjunction with elastic stress distributions (Eqs. 18 and 19). Figure 12(a) shows the result for the slope with $L_t = 0.7 H_t$ and deep-scouring. It can be seen that FS_b dropped drastically and ultimately controlled the

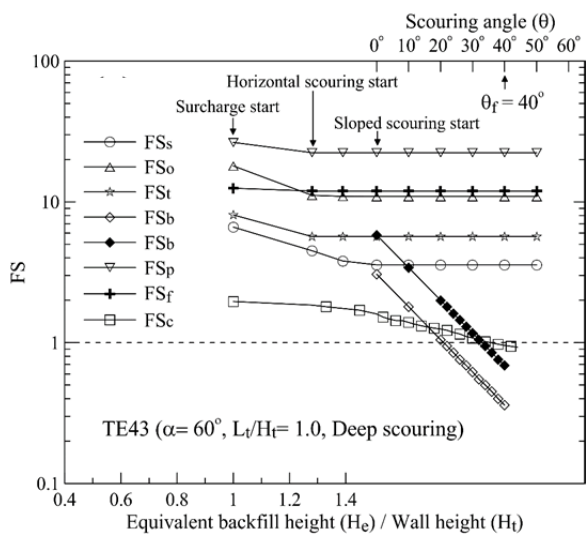
failure of the slope subjected to deep scouring. Figure 12(a) also shows that the intersection between lines of FS_b and $FS = 1.0$ fall in the range of $\theta = 20 \sim 30^\circ$ which slightly underestimated the observed value of $\theta_f = 40^\circ$. A similar prediction for the failure condition ($\theta = 30^\circ$) is also derived based on circular failure analyses (FS_c). Figure 12(b) shows that for shallow scouring, the circular failure analysis (FS_c) outperformed the bearing capacity analysis (FS_b), and rendered a predicted value of $\theta_f \cong 60^\circ$ which is comparable with the measured value of $\theta_f = 57^\circ$. Figure 12(c) shows that the circular failure analysis predicted a failure angle of $\theta_f = 37^\circ$ which is close to the measured value of $\theta_f = 40^\circ$. Figure 12(c) also shows that the upper bound line of FS_b also predicted $\theta_f = 37^\circ$ suggesting that bearing capacity and circular analyses are equally useful for the stability calculations in the case of deep-scouring. However, this is not true for the case of shallow scouring as shown in Fig. 12(d) which indicated that only the circular failure analysis can provide a predicted value of θ_f which is comparable with the measured $\theta_f = 69^\circ$.



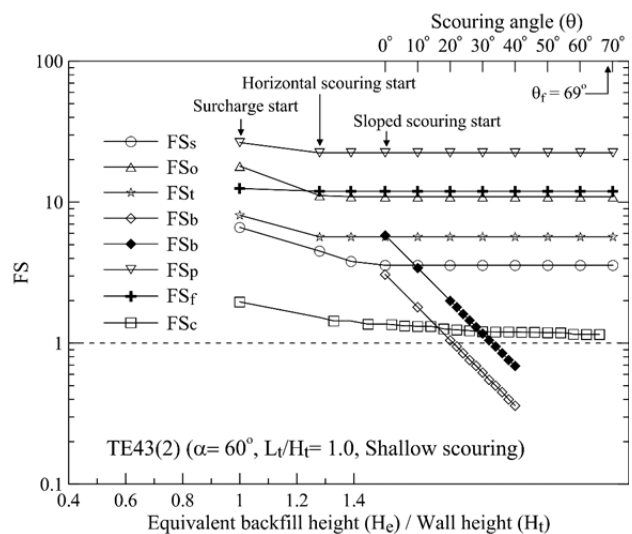
(a) TE30; $L_t / H_t = 0.7$, deep-scouring



(b) TE30(2); $L_t / H_t = 0.7$, shallow-scouring



(c) TE43; $L_t / H_t = 1.0$, deep-scouring



(d) TE43(2); $L_t / H_t = 1.0$, shallow-scouring

Fig. 12 Variations of safety factors during surcharging and toe scouring

The delayed total collapse in the case of shallow scouring (at $\theta_f = 57^\circ$ and 69° in Figs. 12(b) and 12(d), respectively) than those for deep-scouring (at $\theta_f = 40^\circ$ in Figs. 12(a) and 12(c)) is due to: (1) a local bearing capacity failure (under the base of facing) occurred in the case of shallow scouring, contradicting to the global (or compound) failure in the case of deep-scouring; (2) a secondary support provided by the pull-out resistance of reinforcement as shown in Figs. 4(a) and 4(b) which is also illustrated by the significantly increased tensile forces at lower layers of reinforcement shown in Figs. 6(a) and 6(b). It is also noted that the safety factor (FS_c) obtained using circular failure analysis is the only indicator capable of detecting different boundary conditions induced by shallow and deep scouring. This is because:

1. Equations of internal stability (Eqs. 3 ~ 5) and external stability of base sliding and overturning (Eqs. 6 ~ 11) are irrelevant to the scoured profile of the foundation.
2. Equations of bearing capacity (Eqs. 12 ~ 19) take into account the influences of foundation slope angle (θ), load inclination (η), and load eccentricity (e). However, the influence of the height of scoured foundation, D_f (see Figs. 2(a) and 2(b)) on the value of q_u is not taken into account.

Although the circular failure analysis is proved useful based on the above-mentioned investigation, this limit-equilibrium method requires input reinforcement force as an essential input parameter. In the present study, an averaged value of the measured maximum tensile forces (Figs. 6(a) and 6(b)) was used as the input reinforcement force ($T_i = 0.45$ kN/m). This drawback may be overcome via using a force-equilibrium-based finite displacement method (FFDM) proposed by Huang (2014) in which the reinforcement force is a part of the output rather than an input.

11. CONCLUSIONS

Limit equilibrium analyses were performed to evaluate the stability of reinforced slopes at various stages of scoured toe conditions. The process of toe scouring was simulated by removing the backfill horizontally at the passive zone, followed by steepening the foundation ground in front of the slope toe. Results of analyses suggested that bearing capacity and circular failures are dominant failure mechanisms for the slope reinforced with uniform reinforcement lengths of $L_r = 0.7$ and $1.0 H_r$ (H_r : height of reinforced slopes). It was found that results of current internal stability (pull-out, tie-break and facing connections) and external stability (base sliding and overturning) analyses responded insensitively to the boundary changes induced by the toe scouring. The circular failure analysis using a slice method is useful for evaluating the stability status changes of reinforced slopes induced by deep and shallow foundation scouring, provided that adequate input values for the reinforcement force are used. Although the bearing capacity analysis was incapable of detecting the difference between shallow and deep scouring, it was potentially useful for predicting bearing capacity failures for the slopes subjected to deep-scouring.

REFERENCES

- El-Emam, M.M. and Bathurst, R.J. (2004). "Experimental design, instrumentation and interpretation of reinforced soil wall response using a shaking table." *International Journal of Physical Modelling in Geotechnics*, **4**, 13–32.
- El-Emam, M.M. and Bathurst, R.J. (2007). "Influence of reinforcement parameters on the seismic response of reduced-scale reinforced soil retaining walls." *Geotextiles and Geomembranes*, **25**, 33–49.
- Guadagno, F.M., Forte, R., Revellino, P., Fiorillo, F., and Focareta, M. (2005). "Some aspects of the initiation of debris avalanches in the Campania region: The role of morphological slope discontinuities and the development of failure." *Geomorphology*, **66**, 237–254.
- Hansen, J.B. (1970). "A revised and extended formula for bearing capacity." *Danish Geotechnical Institute, Copenhagen*, Bul. 28, 21.
- Huang, C.-C. (1998). "Investigation of the local strains in a geosynthetic composites." *Geotextiles and Geomembranes*, **16**(3), 175–193.
- Huang, C.-C. (2005). "Seismic displacements of soil retaining walls situated on slope." *Journal of Geotechnical and Geoenvironmental Engineering*, ASCE, **131**(9), 1108–1117.
- Huang, C.-C. (2014). "Force-equilibrium-based finite displacement analyses for reinforced slopes: Formulation and verification." *Geotextiles and Geomembranes*, **42**(4), 394–404.
- Huang, C.-C. (2015). "Settlement of footings at the crest of reinforced slopes subjected to toe unloading." *Geosynthetics International*, published on-line, DOI: <http://dx.doi.org/10.1680/jgein.15.00045>.
- Huang, C.-C. and Chen, Y.-H. (2004). "Seismic stability of soil retaining walls situated on slope." *Journal of Geotechnical and Geoenvironmental Engineering*, ASCE, **130**(1), 45–57.
- Huang, C.-C. and Chen, Y.-S. (2012a). "Stability analyses of reinforced walls subjected to simulated toe scouring." *Geosynthetics International*, **19**(4), 284–291.
- Huang, C.-C. and Chen, Y.-S. (2012b). "Behavior of reinforced structures under simulated toe scouring." *Geosynthetics International*, **19**(4), 272–283.
- Huang, C.-C., Hsieh, H.-Y., and Hsieh, Y.-L. (2014). "Hyperbolic models for a 2-D backfill and reinforcement pullout." *Geosynthetics International*, **21**(3), 168–178.
- Huang, C.-C. and Kang, W.-W. (2008). "Seismic bearing capacity of a rigid footing adjacent to a cohesionless slope." *Soils and Foundations*, **48**(5), 641–651.
- Huang, C.-C., Matsushima, K., Mohri, Y., and Tatsuoka, F. (2008). "Analysis of sand slopes stabilized with facing of soil bags with extended reinforcement strips." *Geosynthetics International*, **15**(4), 232–245.
- Miyata, Y., Bathurst, R.J., and Miyatake, H. (2015). "Performance of three geogrid-reinforced soil walls before and after foundation failure." *Geosynthetics International*, **22**(5), 311–326. DOI: <http://dx.doi.org/10.1680/jgein.15.00014>.
- Kuwano, J., Miyata, Y., and Koseki, J. (2014). "Performance of reinforced soil walls during the 2011 Tohoku earthquake." *Geosynthetics International*, **21**(3), 179–196. DOI: <http://dx.doi.org/10.1680/jgein.14.00008>.
- Meyerhof, G.G. (1963). "Some recent research on the bearing capacity of foundations." *Canadian Geotechnical Journal*, **1**(1), 16–26.
- Tatsuoka, F., Tateyama, M., Mohri, Y., and Matsushima, K. (2007). "Remedial treatment of soil structures using geosynthetic-reinforcing technology." *Geotextiles and Geomembranes*, **25**(4-5), 204–220.
- Terzaghi, K. (1943). *Theoretical Soil Mechanics*. John Wiley and Sons, Inc., New York, N.Y.

- Vesic, A.S. (1973). "Analysis of ultimate loads of shallow foundations." *Journal of the Soil Mechanics and Foundations Division: Proceedings of the American Society of Civil Engineers*, **99**(1), 45–73.
- Vesic, A.S. (1975). *Foundation Engineering Handbook*, Chap. 3, 1st ed., eds. Winterkorn, H. F. and Fang, H.Y., Van Nostrand Reinhold, New York, 751.
- Yamaguchi, S., Yanagisawa, M., Uematsu, Y., Kawabe, S., Tatsuoka, F., and Nihei, Y. (2012). "Experimental evaluation of the stability of GRS coastal dyke against over-flowing tsunami." *Proc. 47th Japan National Conference on Geotechnical Engineering*, 1809–1810.
- Kuwano, J., Miyata, Y., and Koseki, J. (2014). "Performance of reinforced soil walls during the 2011 Tohoku earthquake." *Geosynthetics International*, **21**(3), 179–196. DOI: <http://dx.doi.org/10.1680/gein.14.00008>.
- Yamaguchi, S., Yanagisawa, M., Uematsu, Y., Kawabe, S., Tatsuoka, F., and Nihei, Y. (2012). "Experimental evaluation of the stability of GRS coastal dyke against over-flowing tsunami." *Proc. 47th Japan National Conference on Geotechnical Engineering*, pp. 1809–1810.